RAA 2021 Vol. **21** No. **9**, 221(8pp) doi: 10.1088/1674-4527/21/9/221

http://www.raa-journal.org *http://iopscience.iop.org/raa*

***R**esearch in*
***A**stronomy and*
***A**strophysics*

A novel high precision Doppler frequency estimation method based on the third-order phase-locked loop

Tao Deng[1,2⋆], Mao-Li Ma[1], Qing-Hui Liu[1⋆] and Ya-Jun Wu[1]

[1] Shanghai Astronomical Observatory, Chinese Academy of Sciences, Shanghai 200030, China; *liuqinghui@shao.ac.cn, 18811657138@163.com*
[2] University of Chinese Academy of Sciences, Beijing 100049, China

Received 2020 March 6; accepted 2021 April 26

Abstract In deep space exploration, many engineering and scientific requirements require the accuracy of the measured Doppler frequency to be as high as possible. In our paper, we analyze the possible frequency measurement points of the third-order phase-locked loop (PLL) and find a new Doppler measurement strategy. Based on this finding, a Doppler frequency measurement algorithm with significantly higher measurement accuracy is obtained. In the actual data processing, compared with the existing engineering software, the accuracy of frequency of 1 second integration is about 5.5 times higher when using the new algorithm. The improved algorithm is simple and easy to implement. This improvement can be easily combined with other improvement methods of PLL, so that the performance of PLL can be further improved.

Key words: Doppler frequency measurement: deep space exploration: carrier tracking: phase locked loop: high precision

1 INTRODUCTION

Doppler frequency can be used for velocity measurement in deep space exploration. With the development of deep space exploration, the missions of deep space exploration become more and more diverse, which requires higher precision in various Doppler frequency measurement methods (Dong et al. 2018). On the other hand, the study of planetary science also needs higher precision Doppler measurement methods. Taking interplanetary scintillation research as an example, when the electromagnetic wave of the detector passes through the solar wind, various particles in the solar wind will cause the occurrence of the random fluctuation of the amplitude and phase of the electromagnetic wave. Therefore, by measuring the frequency and phase of the electromagnetic wave passing through the solar wind, the density, wind speed and structure of the plasma in the solar wind can be deduced (Ma et al. 2016).

Phase-locked loop (PLL) is an algorithm that is able to measure the Doppler frequency and phase. The error of PLL is mainly divided into two parts: one is the random error (mainly caused by thermal noise and oscillator noise) and the other is the steady-state error, that is, the dynamic stress error. In a general PLL, these two errors are usually controlled by the noise bandwidth of the loop. However, when the bandwidth of loop noise is reduced, the dynamic stress error increases even though the random noise is suppressed, and vice versa (Mao et al. 2004a; Li et al. 2016). In view of this contradiction, Mao et al. (2004b) proposed a technique of adding a fuzzy controller in PLL to adaptively adjust the loop bandwidth, so as to minimize the phase and frequency tracking error of the PLL while ensuring that the loop does not lose lock. In Ren et al. (2014), Liu et al. (2013) and Kou & Zhang (2016), prior information is used to dynamically compensate the signal as far as possible, so that smaller loop noise bandwidth can be used to track the signal and the total phase and frequency tracking errors can be reduced. Further, linear Kalman filter (LKF) (Miao et al. 2009), extended Kalman filter (EKF) (Xu et al. 2012; Tang et al. 2013; Jwo 2001) or unscented Kalman filter (UKF) (Han et al. 2010) is also used for performance improvements in the PLL. To some extent, the tracking accuracy and weak signal detection capability of PLL are improved, but its computational complexity increase obviously. In Li et al. (2011), wavelet packet de-noising technique is applied to PLL, which also improves the tracking accuracy and allows broadening the PLL bandwidth. Li et al. (2016) proposed a strategy

⋆ Corresponding author

to estimate the steady-state phase error and compensate the tracking result. When the noise bandwidth of the phase-locked loop is small, the method can significantly reduce the dynamic stress error of the phase-locked loop and enhance the tracking ability of the transient phase change of the phase-locked loop. However, when the noise bandwidth of the loop is large, even the dynamic stress error is inversely proportional to the noise bandwidth of the loop, more random errors are introduced in the compensation process of dynamic stress error, and the total phase measurement accuracy of the PLL is slightly decreased.

In Planetary Radio Interferometry and Doppler Experiment (PRIDE) of Joint Institute for Very Long Baseline Interferometry (VLBI) in Europe, phase-locked loop is used as the basic technical unit of measuring signal's phase and frequency in carrier tracking (Duev et al. 2016). Shanghai Astronomical Observatory also developed a Doppler frequency measurement software based on second-order Costas phase locked loop, and compared the results with PRIDE's processing results in the measurement of interplanetary scintigraphy, it was found that the frequency and phase measurement results of the two software were highly consistent (Ma et al. 2016).

In order to further improve the tracking accuracy of Doppler frequency, we analyze the available output positions of the frequency in third-order Costas PLL, and propose a new measurement method of Doppler frequency. The simulation and real data processing show that the new algorithm has a strong ability to suppress random noise.

The innovation points of this paper are as follows: first, the positions of the third-order PLL, which can be used as Doppler frequency output, are pointed out, and the similarities and differences between the two Doppler frequency measurement schemes are compared. Second, a kind of high precision Doppler frequency method is proposed based on the first discovery.

The first section of this paper is introduction about PLL and related technical improvement. The second section is to give the concrete realization structure diagram of the classical third-order Costas PLL and different measurement schemes of Doppler frequency based on the third-order PLL. In the third section, by analyzing the simulation data, the differences between the improved PLL algorithm and the traditional third order PLL algorithm in accuracy of Doppler frequency measurement are compared. In the fourth section, some real data were processed. The fifth section presents the summary and the work outlook.

2 IMPLEMENTATION OF HIGH PRECISION PHASE-LOCKED LOOP ALGORITHM

2.1 Output Positions of Doppler Frequency in Third-order Costas PLL

Figure 1 shows the structure of Costas PLL adopted by the classical Doppler frequency measurement software. Loop filter is JR (Jaffe-Rechtin) filter which is designed according to Minimum Mean Square Error (MMSE). The transformation between continuous system and discrete system is given by Tian et al. (2016)

$$\frac{1}{s} = \frac{Tz^{-1}}{1 - z^{-1}}\,. \tag{1}$$

The discrete structure used to analyze the third-order phase-locked loop is shown in Figure 2, where T is integrate and dump period and also is loop updating time. The function of the integrate and dump filter is to accumulate the data with time length T into a point as output. In Figure 2, there are two output positions of measured frequency. If w_1 is selected as the output position of Doppler frequency, the frequency of signal measured by PLL can be expressed as

$$f_1 = \frac{w_1}{2\pi}\,. \tag{2}$$

If w_2 is selected as the output position of Doppler frequency, then the output frequency can be expressed as

$$f_2 = \frac{w_2}{2\pi T}\,. \tag{3}$$

For the case of using w_1 as the output position of frequency, the discrete structure in Figure 2 is converted into the corresponding continuous form, as shown in Figure 3.

In Figure 3, $\widehat{\theta}_1$ is the measured phase, $\Delta\theta_1$ is the error signal. Its error transfer function is

$$\phi_{1e}(s) = \frac{2w_n^2 s + w_n^3}{s^3 + 2w_n s^2 + 2w_n^2 s + w_n^3}\,. \tag{4}$$

When the input signal phase is a parabolic signal $\theta(t) = 0.5at^2$, the steady-state error of the measured phase is

$$\Delta\theta_1(\infty) = \lim_{s\to 0} s \cdot \frac{a}{s^3}\phi_{1e}(s) = \frac{2a}{w_n^2}\,. \tag{5}$$

The steady-state error is a value related to a, indicating that although the system at this time is a third-order system, it cannot track the second-order change of Doppler frequency because it chooses w_1 as the output position of frequency. Therefore, from the perspective of eliminating steady-state error, although the JR filter is a second-order filter, the PLL is still a second-order PLL in this case.

If w_2 is selected as the output Doppler frequency position, the corresponding transfer function block diagram can be shown in Figure 4.

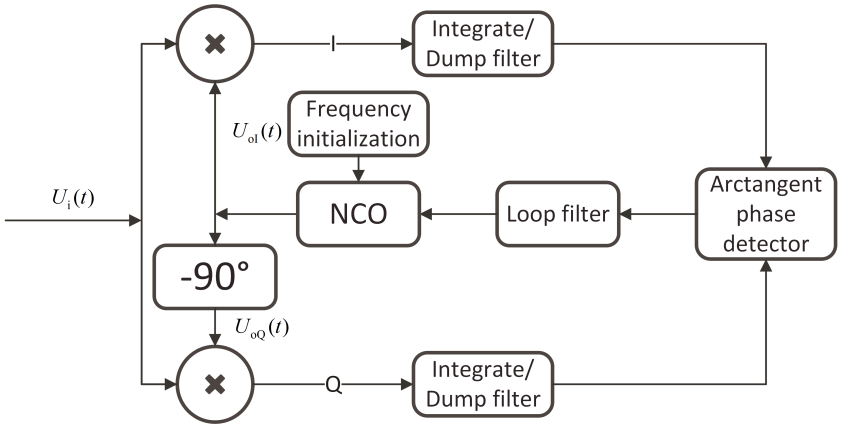

Fig. 1 Costas PLL structure.

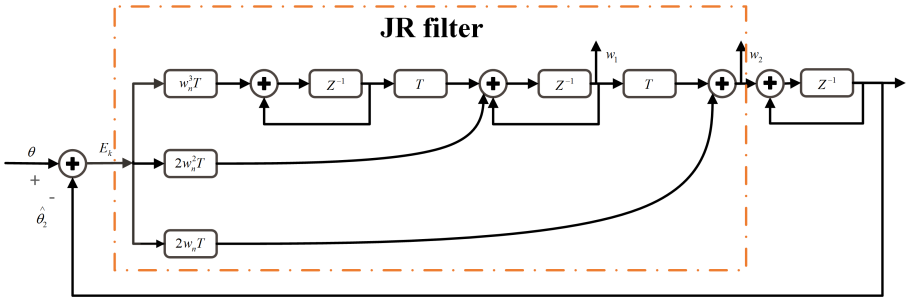

Fig. 2 Linear discrete structure of third order Costas PLL.

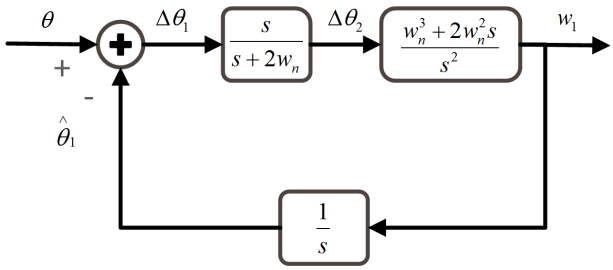

Fig. 3 Structure of third order Costas phase locked loop with w_1 as output position of frequency.

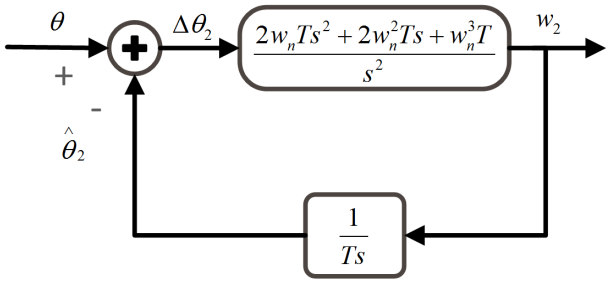

Fig. 4 Structure of third order Costas phase locked loop with w_2 as output position of frequency.

Figures 3 and 4 are equivalent transfer function block diagrams, both of which are continuous representations of the discrete system in Figure 2. In Figure 4, $\widehat{\theta}_2$ is the measured phase, $\Delta\theta_2$ is the error signal of input phase. Its error transfer function is

$$\phi_{2e}(s) = \frac{s^3}{s^3 + 2w_n s^2 + 2w_n^2 s + w_n^3}\,. \tag{6}$$

When the input phase is a parabolic signal $\theta(t) = 0.5at^2$, the steady-state error of the output phase is

$$\Delta\theta_2(\infty) = \lim_{s\to 0} s \cdot \frac{a}{s^3}\phi_{2e}(s) = 0\,. \tag{7}$$

The steady-state error is 0, indicating that the second derivative of Doppler frequency can be tracked when the position w_2 is the output frequency position of the system.

In order to compare the difference between two Doppler frequency measurement strategies in suppressing

random phase noise. It is assumed that the random noise in the input phase can be described as white noise. The power spectrum of the white noise is $S_X(w) = \frac{N_0}{2}$, and N_0 is constant. For the case where w_1 is the measuring point of Doppler frequency, the corresponding noise power transmission function is

$$H_1(w) = |1 - \phi_{1e}(jw)|^2 . \tag{8}$$

Then the output power spectrum of the noise after passing through the system is

$$S_{Y1}(w) = H_1(w)S_X(w) . \tag{9}$$

Finally, the average noise power of the output is

$$\begin{aligned} E[Y_1^2(t)] &= R_{Y1}(0) = \frac{1}{2\pi}\int_{-\infty}^{\infty} S_{Y1}(w)e^{jw\tau}dw|_{\tau=0} \\ &= \frac{1}{2\pi}\int_{-\infty}^{\infty} H_1(w)S_X(w)e^{jw\tau}dw|_{\tau=0} = \frac{1}{2}w_nN_0. \end{aligned} \tag{10}$$

Similarly, for the case where w_2 is the measuring point of Doppler frequency, the average noise power of the output is

$$E[Y_2^2(t)] = \frac{5}{6}w_nN_0 . \tag{11}$$

$E[Y_1^2(t)] < E[Y_2^2(t)]$, it means that for the case where w_1 is the measuring point of Doppler frequency, the measurement results will contain less random noise.

3 PERFORMANCE ANALYSIS

3.1 Dynamic Stress Error

After selecting w_1 as the frequency output position, the analysis of Figure 3 shows that when the phase of the input signal is a parabolic signal, there is a steady-state error between the phase of the input signal and the measured phase. Therefore, when there is a non-negligible second derivative of Doppler frequency, the measurement results will introduce a large dynamic stress error, resulting in a serious decline in tracking accuracy.

For the Doppler frequency and phase measurement method shown in Figure 3, when the input phase signal is $\theta(t) = \frac{1}{6}bt^3$, the Laplace transform of the input phase signal is $\Theta(s) = \frac{b}{s^4}$. Then the Laplace transform of the phase difference $\Delta\theta_1$ is

$$\begin{aligned} \Delta\Theta(s) &= \Theta(s)\phi_{1e}(s) \\ &= \frac{b(s+2w_n)}{s^5 + 2w_ns^4 + 2w_n^2s^3 + w_n^3s^2} . \end{aligned} \tag{12}$$

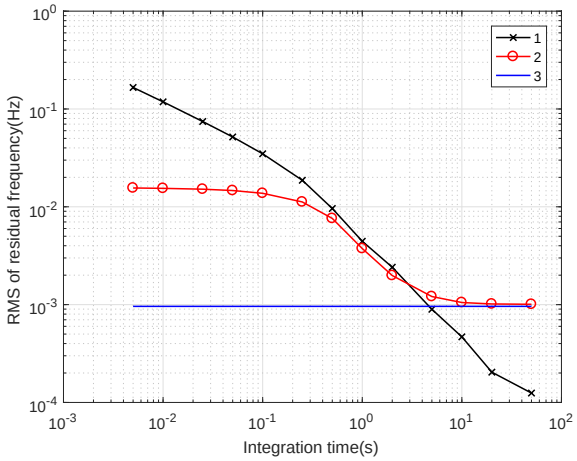

Fig. 5 The RMS of residual Doppler frequencies and abscissa represents the integration time of the measured frequency. The residual frequency is obtained by subtracting the measured frequency from the real frequency. Loop updating time is 5ms. Label 1 represents the results obtained from PLL with w_2 as frequency output position, label 2 represents the results obtained from PLL with w_1 as frequency output position. Label 3 represents dynamic stress error in this case. Loop noise bandwidth is set to $4.17\,\mathrm{Hz}$ when the PLL tracks frequency stably. Set $f_0 = 1\,\mathrm{MHz}$, $f_1 = 300\,\mathrm{Hz\,s^{-1}}$, $f_2 = 0.012\,\mathrm{Hz\,s^{-2}}$, $\varphi = 0$.

The time domain expression of the phase difference $\Delta\theta_1$ can be expressed as

$$\begin{aligned} \Delta\theta_1 = b(&\frac{2t}{w_n^2} - \frac{3}{w_n^3} + \frac{e^{-w_nt}}{w_n^3} \\ &+ \frac{2\cos(\frac{\sqrt{3}w_nt}{2})e^{-\frac{w_nt}{2}}}{w_n^3}) . \end{aligned} \tag{13}$$

In practice, we often set $w_n > 0.5$, then with the increase of t, e^{-w_nt} and $e^{\frac{-w_nt}{2}}$ gradually decrease to 0, and $|\cos(\frac{\sqrt{3}w_nt}{2})| \leq 1$. Therefore, when the PLL stably tracks the signal, the time-domain expression of the phase difference is simplified to

$$\Delta\theta_1(t) = b(\frac{2t}{w_n^2} - \frac{3}{w_n^3}) . \tag{14}$$

In this case, the phase difference of the main loop is the ramp signal, and the second and higher derivatives of the phase difference are 0. The derivative of $\Delta\theta_1(t)$ with respect to time is the dynamic stress error of angular frequency, which can be expressed as

$$\Delta\omega = \frac{2b}{w_n^2} . \tag{15}$$

Equation (15) will be used for accuracy analysis in simulation.

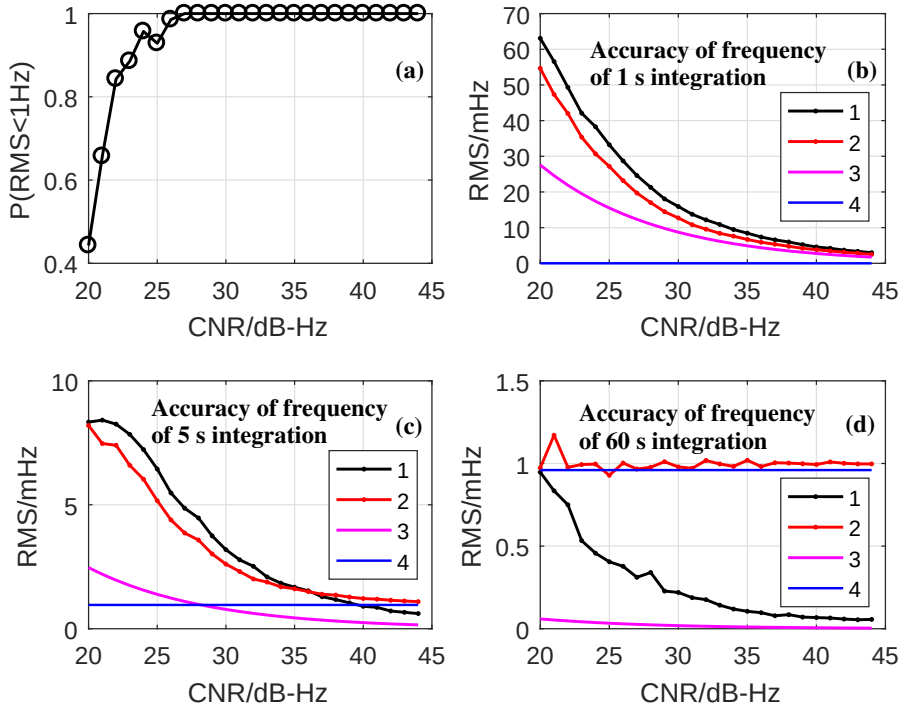

Fig. 6 Probability of frequency being locked correctly and RMS of residual frequency under different CNRs. P represents the probability of frequency being locked correctly. When analyzing P under different CNRs, 100 Monte Carlo trials were conducted for each fixed CNR and the RMS of residual frequency less than 1Hz was believed to be correct. Label 1 represents the results obtained from PLL with w_2 as frequency output position, label 2 represents the results obtained from PLL with w_1 as frequency output position. Label 3 represents optimal tracking accuracy of frequency which is square root of CRLB. Label 4 represents dynamic stress error of frequency in this case. Set $f_0 = 1\,\text{MHz}$, $f_1 = 300\,\text{Hz s}^{-1}$, $f_2 = 0.012\,\text{Hz s}^{-2}$, $\varphi = 0$. Loop updating time is $5\,\text{ms}$.

3.2 Cramer-Rao Lower Bound (CRLB) of Frequency Estimation

The observation data are expressed as

$$X[n] = A\cos(\omega n + \phi) + \lambda[n], \quad n = 0, 1, \cdots, N-1, \tag{16}$$

where A is amplitude, ω is frequency with unit rad, ϕ is intial phase, and N is the number of sampling points independently. $\lambda[n]$ is Gaussian white noise whose mean is 0 and variance is σ^2. In a phase-locked loop, the amplitude and the initial phase hardly affect the estimation accuracy of frequency, so when calculating the CRLB, it can be considered that the amplitude and the initial phase are known. If ω is total unknown, then the CRLB of ω (Zhu 2015) is

$$var(\omega - \widehat{\omega}) \geq \frac{\sigma^2}{A^2}\frac{12}{N(N-1)(2N-1)}. \tag{17}$$

$\widehat{\omega}$ is the estimated value of ω. The optimal root mean square(RMS) of the estimated carrier frequency, that is square root of CRLB, can be calculated

$$\begin{aligned} rms(f_c - \widehat{f_c}) &= f_s\frac{\sqrt{var(\omega - \widehat{\omega})}}{2\pi} \\ &\geq f_s\sqrt{\frac{\sigma^2}{A^2}\frac{3}{\pi^2 N(N-1)(2N-1)}}. \end{aligned} \tag{18}$$

f_c is carrier frequency of input signal with unit Hz, $\widehat{f_c}$ is the estimated value of f_c. f_s is sampling rate of input signal. The square root of CRLB can be used as an absolute standard to evaluate the tracking accuracy of measured frequency.

3.3 Accuracy Analysis of Measured Frequency

Simulation parameters: sampling rate $f_s = 4\,\text{MHz}$, total time of signal is $305\,\text{s}$. White Gaussian noise is added, and set carrier to noise ratio CNR$= 40\,\text{dB-Hz}$. CNR is defined as

$$\text{CNR} = 10\log_{10}(\frac{P_s}{N_0}) = 10\log_{10}(\frac{A^2}{2\sigma^2 T_s}). \tag{19}$$

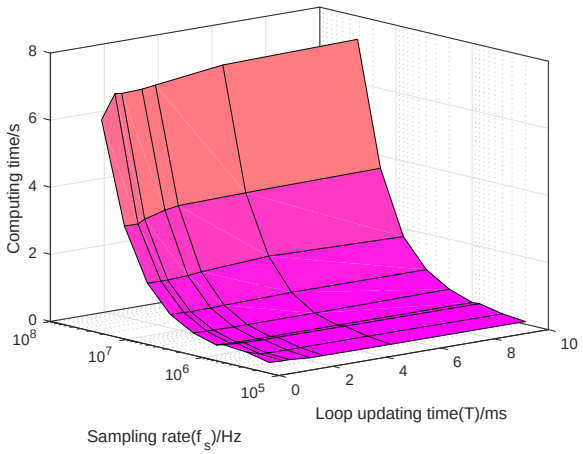

Fig. 7 Computing time is shown when processing 1 second data and the algorithm is achieved in Matlab language.

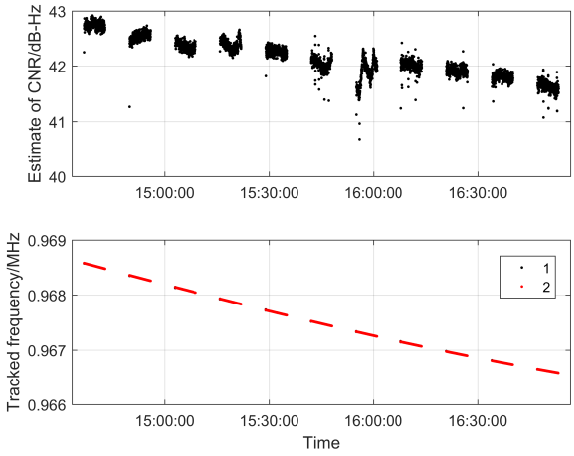

Fig. 8 The estimated CNR and measured frequency. Label 1 represents the measured frequency f_2 which is obtained by using PLL in which w_2 as the output position of frequency. Label 2 represents the measured frequency f_1 which is obtained by using PLL in which w_1 as the output position of frequency.

In which P_s is the signal power and N_0 is the noise spectral density, and σ^2 is the noise variance and T_s is sampling period of input signal.

The phase of input signal is defined as

$$\theta(t) = \varphi + 2\pi f_0 t + 2\pi \frac{f_1}{2} t^2 + 2\pi \frac{f_2}{6} t^3 \,. \qquad (20)$$

φ is the initial phase. The units of f_0, f_1, f_2 are Hz, Hz s^{-1}, Hz s^{-2}, respectively.

When setting the noise bandwidth of the loop, considering the need to reduce the adjustment time and guarantee the tracking accuracy at the same time, the bandwidth can be decreased gradually from a large value to a small value in a small period of time at the beginning of the tracking, and then remain constant (Yan et al. 2015). In this simulation, the loop noise bandwidth was set to decrease gradually from 20.83 Hz to 4.17 Hz (ω_n decreases from 25 to 5) in the first 5 seconds.

Figure 5 shows the accuracy of frequency under different integration time. Under the current parameter setting conditions, when the integration time of frequency is less than 3 seconds, the new algorithm can improve the tracking accuracy of frequency. Moreover, the shorter the integration time is, the more significant the improvement of tracking accuracy of the new algorithm is. However, when the integration time is larger than 3 seconds, the tracking accuracy of the new algorithm is not as good as that of the original algorithm. With the increase of integration time, the tracking accuracy of the new algorithm almost does not improve and approaches the dynamic stress error.

The analysis of the above results shows that in the frequency of short time integration, random noise is dominant, and the dynamic stress error is relatively small. Compared with the original algorithm, the order of the phase-locked loop of the new algorithm is reduced by one order, and the ability to suppress the dynamic stress error is poor. However, the new algorithm has strong random noise suppression ability, so the total noise of the Doppler frequency of the short-period integral obtained by new algorithm is still significantly less than that of the original algorithm. With the increase of integration time, the random noise is suppressed, and then the dynamic stress error of frequency starts to dominate. Due to the poor ability of the new algorithm to suppress the dynamic stress error, the total error of the new algorithm is larger than that of the original algorithm. To sum up, the new algorithm has obvious advantages in the frequency measurement of short time integration, while the traditional method has advantages in the frequency measurement of long time integration. In fact, when the external force on the probe is very small, such as during the flight of the Mars probe to Mars, the third order term of the phase can be ignored. At this point, the new algorithm still has advantages in frequency measurement of long time integration.

Figure 6(a) shows the probability that the PLL can track the frequency correctly when the general parameters are set and the signal is set with a large dynamic. It can be seen that the PLL can track the frequency of the signal stably when the CNR is larger than 26 dB-Hz, which meets the requirements of carrier tracking for probes in most cases. Figure 6(b), (c) and (d) illustrate that in the case that the integration time of frequency is short enough and the CNR is low enough, the random error of the measured frequency is dominant, then the new algorithm can be used to improve the tracking accuracy of frequency. On the contrary, when the integration time of frequency is long enough or the CNR is high

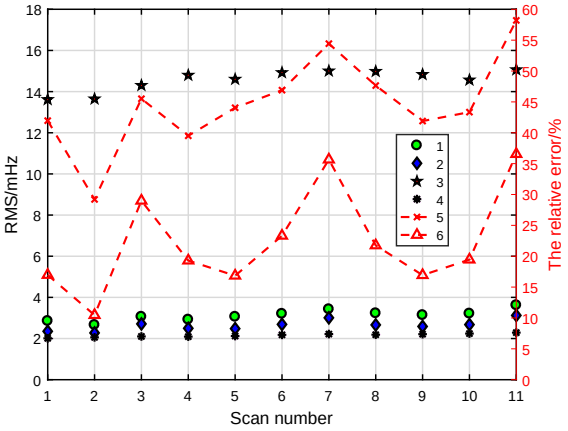

Fig. 9 The comparison of the accuracy of measured frequency obtained by different methods. Label 1 represents the accuracy of measured frequency f_2 which is obtained by using PLL in which w_2 as the output position of frequency. Label 2 represents the accuracy of measured frequency f_1 which is obtained by using PLL in which w_1 as the output position of frequency. Label 3 represents the accuracy of measured frequency obtained by using Doppler software (Zheng et al. 2013) which has been used in carrier tracking in recent deep space exploration missions. Label 4 represents the theoretical optimal accuracy which is square root of CRLB. Label 5 represents the relative error between the accuracy of f_2 and square root of CRLB. Label 6 represents the relative error between the accuracy of f_1 and square root of CRLB.

enough, the dynamic stress error is dominant in the measured frequency, then the original algorithm can be used to achieve higher precision frequency measurement. In practical applications, combining the advantages of the two algorithms in frequency measurement, the PLL can achieve better tracking performance for frequency.

3.4 Computing Time

In the PLL presented in this paper, there are two parameters that affect the computing time of the algorithm. The two parameters are the sampling rate of input data f_s and loop updating time T, respectively. Figure 7 shows the computing time of PLL at different f_s and T. The f_s set during simulation basically cover the values of sampling rate of recorded data which is commonly used in deep space exploration. At the same time, T is also a typical value in practical engineering applications. The smaller the value of T is, the high-dynamic tracking ability of the algorithm will be improved, but at the same time, the weak signal tracking ability will become worse. The value of T can be determined according to the actual demand. For example, the smaller T is, the better it is to accurately analyze the time when the probe crashes onto the moon, on the premise that the algorithm correctly tracks the frequency.

4 ACTUAL DATA PROCESSING

The observation data of Longjiang-2 minor satellite with 2-bits sampling were recorded in Shanghai very long baseline interferometry(VLBI) data processing center, and the sampling rate and bandwidth of recorded data are 4 MHz and 2 MHz, respectively. When tracking frequency, set the loop bandwidth to 4.17 Hz when loop becomes stable. These data were observed by Urumuqi (UR) station of Chinese VLBI network on 2018 August 24. In observation, the VLBI station alternate observations of radio source and Longjiang-2.

When estimating the CNR of data, phase stopping (Duev et al. 2016) is used to concentrate the energy of the signal within 1 Hz. The maximum amplitude of the power spectrum of data per second is taken as the signal power and take the mean value of some amplitude values except the maximum value in the power spectrum as estimated noise power. Then CNR is calculated by using Equation (19). The estimated CNR and measured frequency are shown in Figure 8.

From Figure 9, several conclusions can be drawn. First, the third-order PLL with w_1 as the output position of frequency can obtain significantly higher accuracy of frequency compared with the third-order PLL with w_2 as the output position of frequency. Second, the tracking accuracy of frequency of the new method is close to the Cramer-Rao lower bound, which indicates that the frequency estimator obtained by the new method is close to the minimum variance unbiased estimator even if the general parameters are set. Third, the new method can obtain frequency estimates with significantly higher accuracy than the Doppler software used for deep space exploration (Zheng et al. 2013). In addition, the coefficient of the quadratic term is much less than 0.1 mHz s^{-2} when the measured frequency is fitted with a quadratic polynomial, which illustrates that the random error is dominant in the actual data, so the influence of the dynamic stress error on the accuracy of the new algorithm can be ignored.

In addition, data from Chang'e-5 on 2020 November 28 were also processed. The differences between the measured Doppler velocity and the velocity of precision ephemeris obtained by orbit determination are below 15 mm s^{-1}, which further indicates the correctness of the proposed algorithm for frequency measurement.

5 CONCLUSIONS

The improved PLL algorithm chooses w_1 rather than w_2 as the output position of frequency, this frequency

measurement strategy shows a strong ability to suppress random noise. But from the perspective of input steady-state error, although the JR filter is a second-order filter, the PLL is still a second-order PLL in this case. Therefore, when the Doppler phase of the input signal has the third derivative with respect to time that cannot be ignored, there will be a large steady-state error in selecting the Doppler frequency measurement point w_1, which will seriously affect the tracking accuracy of Doppler frequency, especially when setting small loop noise bandwidth.

When the random error of the measured frequency is dominant, such case is often encountered if the integration time of frequency is short enough and the CNR is low enough, then the new algorithm is useful in improving the tracking accuracy of frequency. On the contrary, in the case that the integration time of frequency is long enough or the CNR is high enough, the dynamic stress error is dominant in the obtained frequency, then the original algorithm can be used to achieve higher tracking accuracy of frequency. In practice, combining the advantages of the two algorithms, better tracking performance of frequency can be achieved by PLL.

In fact, in many cases, the third derivative of the phase is very small and can be ignored, which illustrates that the random error is dominant in the actual data. At this point, the new algorithm still has advantages in estimating frequency of long time integration. The improved PLL algorithm is easy to realize and the effect is extremely good.

Acknowledgements The research presented in this paper has been supported by the National Natural Science Foundation of China (Grant Nos. 11773060, 11973074, U1831137 and 11703070), National Key Basic Research and Development Program (2018YFA0404702), Shanghai Key Laboratory of Space Navigation and Positioning (3912DZ227330001) and the Key Laboratory for Radio Astronomy of CAS. Thanks to Li Peijia, associate researcher of Shanghai Observatory, for her help in orbit determination.

References

Dong, G., Li, H., Hao, W., et al. 2018, Journal of Deep Space Exploration, 5, 99 (in Chinese)

Duev, D., Pogrebenko, S., Cimo, G., et al. 2016, A&A, 593, A34

Liu, G., Guo, M., et al. 2013, in Proceedings 2013 International Conference on Mechatronic Sciences, Electric Engineering and Computer (MEC), 2927

Han, S., Wang, W., Chen, X., & Meng, W. 2010, Hangkong Xuebao/Acta Aeronautica et Astronautica Sinica, 31, 2393 (in Chinese)

Jwo, D. J. 2001, IEE Proceedings - Radar, Sonar and Navigation, 148, 241

Li, Y., Xu, X., & Zhang, T. 2011, in CSEE 2011: Advances in Computer Science, Environment, Ecoinformatics, and Education, 214, 449, https://link.springer.com/content/pdf/10.1007%2F978-3-642-23321-0.pdf

Li, Y., Zhang, R., & Jiang, W. 2016, in 2nd IEEE International Conference on Computer and Communications (ICCC), 294

Ma, M. L., Zheng, W. M., Chang, S. Q., & Zhou, W. L. 2016, Scientia Sinica Physica, Mechanica & Astronomica, 46, 77 (in Chinese)

Mao, W.-L., Tsao, H.-W., & Chang, F.-R. 2004a, IEE Proc.-Radar Sonar Navigation, 151, 171

Mao, W.-L., Tsao, H.-W., & Chang, F.-R. 2004b, IEEE Signal Processing Letters, 11, 431

Miao, J., Sun, Y., Liu, J., & Chen, W. 2009, in 2009 Sixth International Conference on Fuzzy Systems and Knowledge Discovery, 4, 438

Ren, C., Liu, Q., Wang, M., & Yang, L. 2014, in Proceedings of the 2014 International Conference on Wireless Communication and Sensor Network, 114

Tang, X., Falco, G., Falletti, E., & Lo Presti, L. 2013, in 2013 International Conference on Localization and GNSS (ICL-GNSS), 1

Tian, T., Cui, C., & Cheng, L.-M. 2016, Space Electronic Technology, 57 (in Chinese)

Xu, Y., Chang, Q., & Yu, Z. 2012, in 2012 2nd International Conference on Consumer Electronics, Communications and Networks (CECNet), 111

Yan, D., Zheng, H., & Chen, Z. 2015, Journal of Telemetry, Tracking and Command, 36, 63 (in Chinese)

Kou, Y., & Zhang, H. 2016, Sensors, 16, 519

Zheng, W., Ma, M., & Wang, W. 2013, Journal of Astronautics, 34, 1462 (in Chinese)

Zhu, L. 2015, Study on Frequency Estimators for noisy Sinusoid Signals, PhD thesis (in Chinese)